Chapter 9: Understanding and Attributing Climate Change

Coordinating Lead Authors: Gabi Hegerl, Francis Zwiers

Lead Authors: Pascale Braconnot, Nathan Gillett, Yong Luo, Jose Marengo, Neville Nicholls, Joyce Penner, Peter Stott

Contributing Authors: M. Allen, C. Ammann, N. Andronova, R. Betts, A. Clement, W. Collins, S. Crooks, T. Delworth, R. van Dorland, C. Forest, P. Forster, H. Goosse, J. Gregory, D. Harvey, F. Joos, G. Jones, J. Kenyon, J. Kettleborough, R. Knutti, H. Lambert, M. Lavine, D. Levinson, V. Masson, T. Nozawa, B. Otto-Bliesner, D. Pierce, S. Power, D. Rind, L. Rotstayn, B. D. Santer, C. Senior, S. Stark, D. Stone, S. Tett, P. Thorne, M. Wang, B. Wielicki, T. Wong, L. Xu, X. Zhang, E. Zorita

Review Editors: David Karoly, Laban Ogallo, Serge Planton

Date of Draft: 12 August 2005

Notes: This is the TSU compiled version

Figures

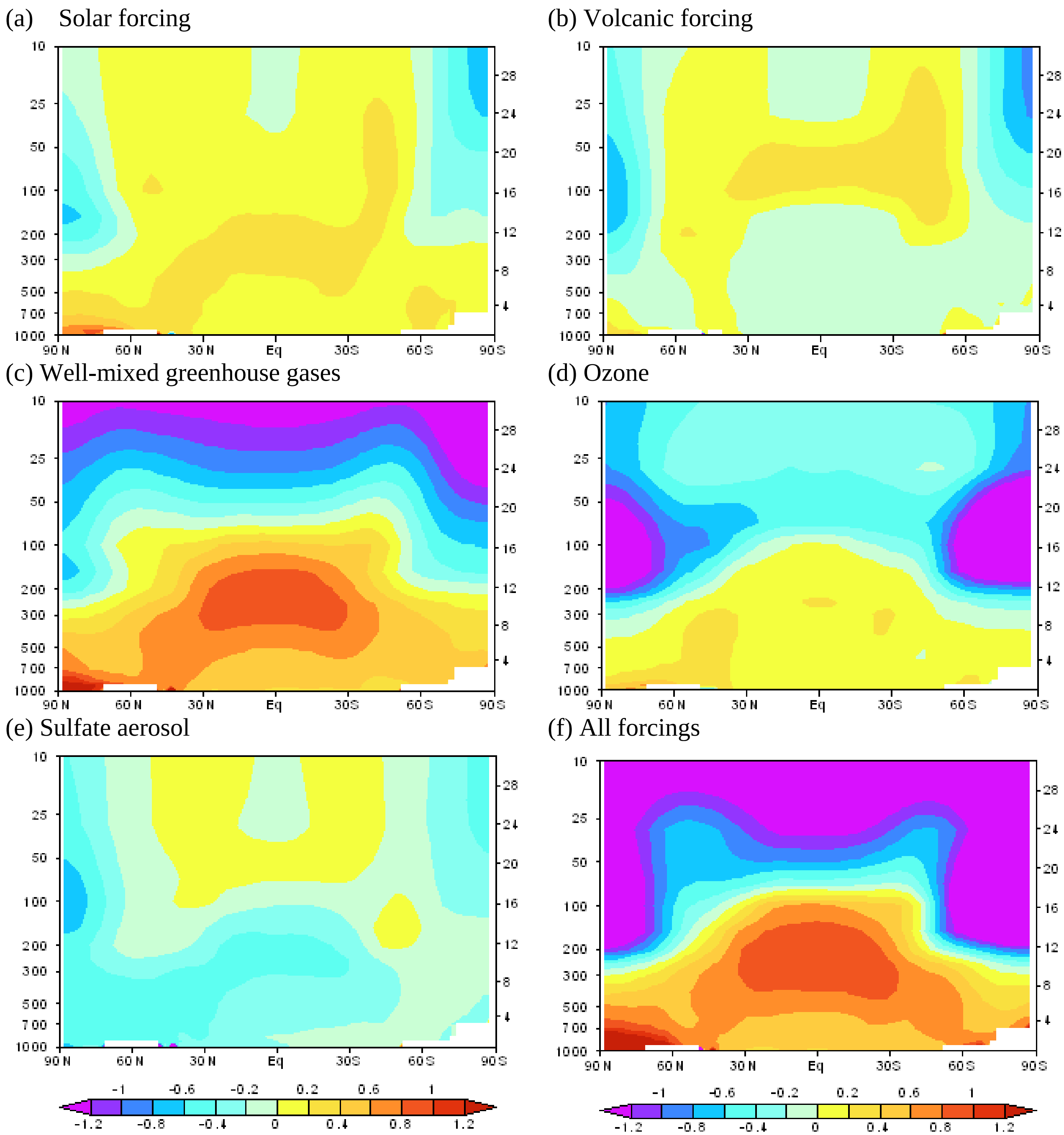

Figure 9.2.1. Zonal mean temperature change during the 20th century (°C/Century) as simulated by the PCM model from (a) solar forcing, (b) volcanoes, (c) well-mixed greenhouse gases, (d) tropospheric and stratospheric ozone changes, (e) direct sulphate aerosol forcing, and (f) the sum of all forcings. Plot is from 75N to 75S and from 1000 hPa to 10 hPa.. Based on Santer et al. (2003b).

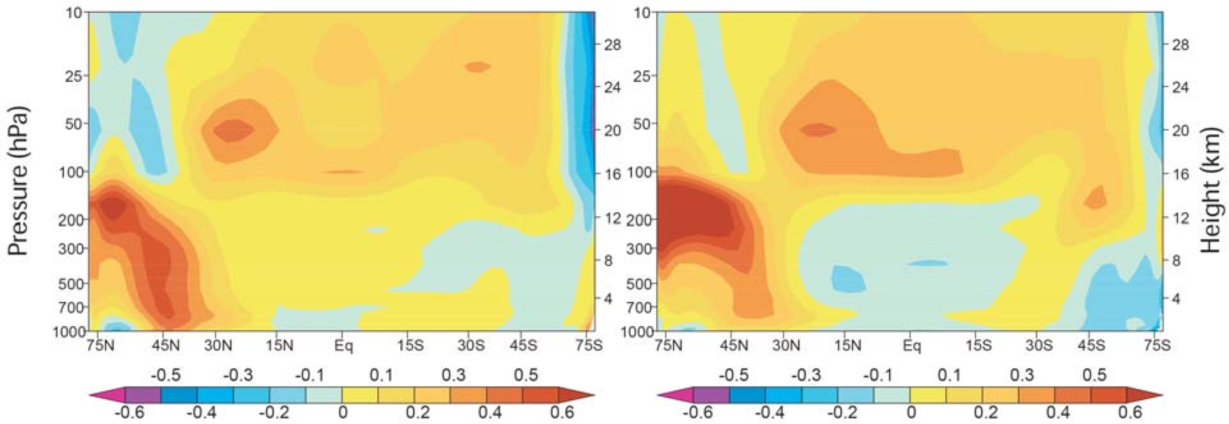

Figure 9.2.2. The response to (a) direct forcing from fossil fuel black carbon and organic matter (BC+OM) and (b) the sum of fossil fuel BC+OM and biomass burning aerosols as simulated by the CSIRO model. Note the difference in colour scale from Figure 9.2.1. Based on Penner et al. (2005).

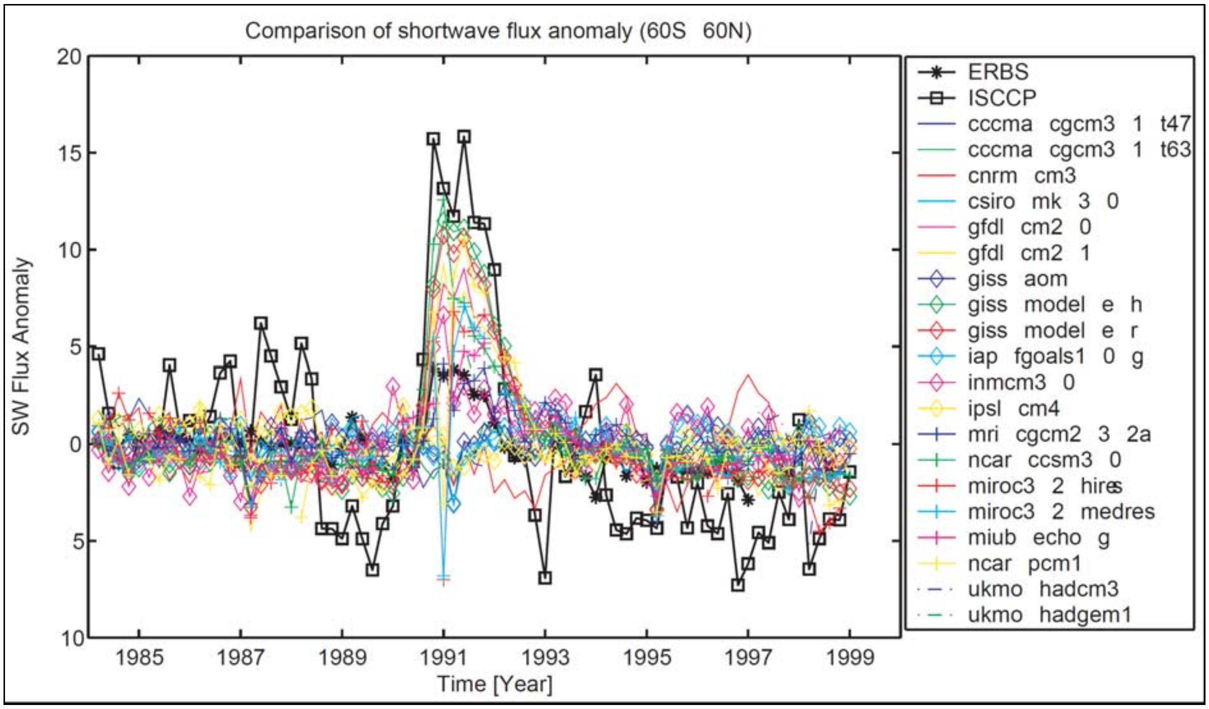

Figure 9.2.3. Comparison of outgoing shortwave flux from AR4 models with ERBS (Wong et al., 2005) and ISSCP (Zhang et al., 2004) satellite data.

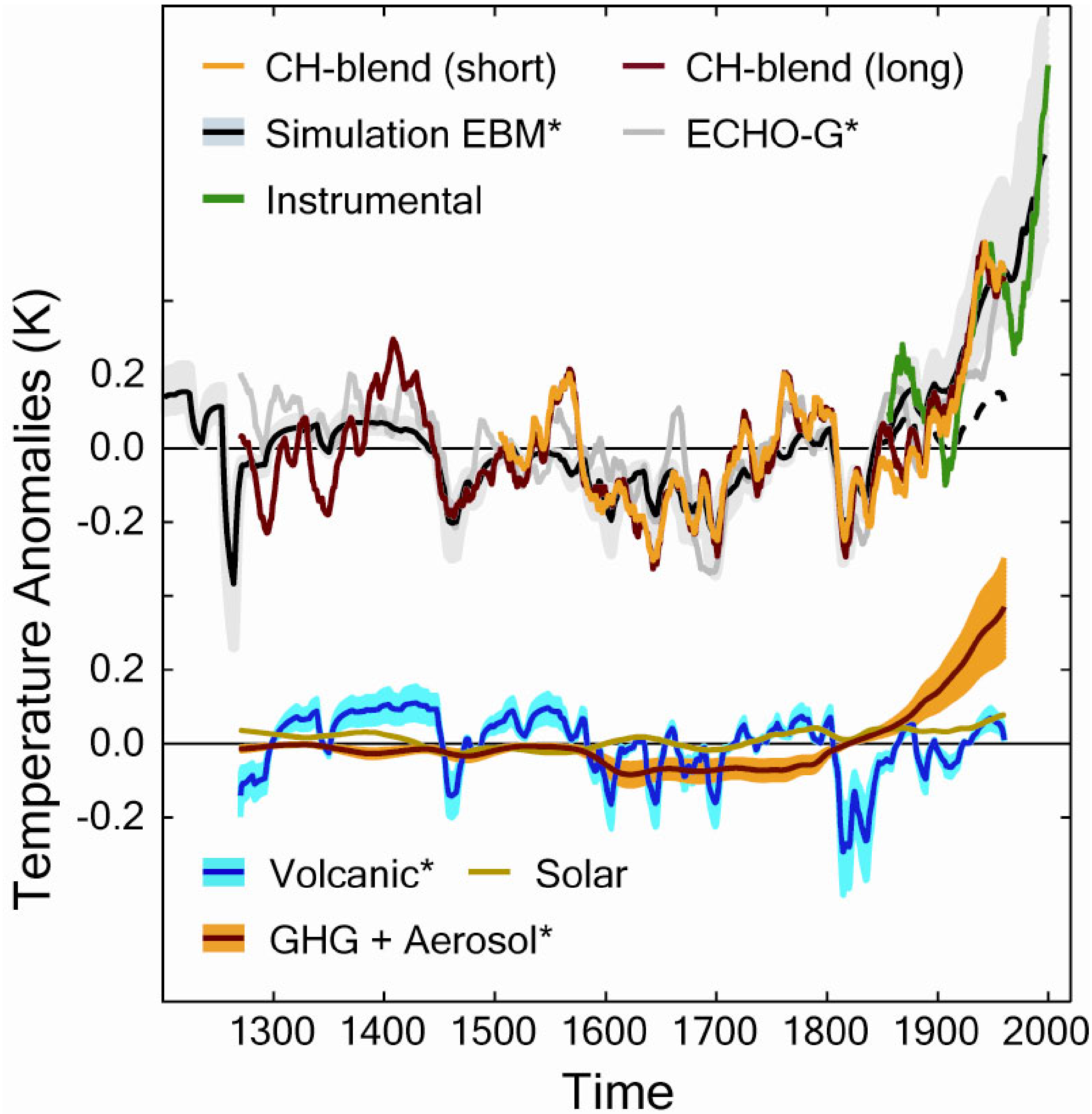

Figure 9.3.1. Detection results for multiple 1k year NH reconstructions. After Hegerl et al. (2003; 2005a). Contribution of external forcing to reconstructed mean temperature north of 30N. The top panel shows the reconstructions and the instrumental record compared to simulations with an Atmosphere-Ocean General Circulation model and an Energy Balance climate model (EBM) forced with estimates of volcanic, solar, and anthropogenic forcing (EBM simulation with natural forcing only in industrial period dashed). The simulations, are scaled to best fit the reconstructions; the agreement is highly significant (less than 5% significance level). The bottom panel shows an estimate of the contribution from individual forcings (volcanism, solar forcing, and greenhouse gas and aerosol forcing combined) and the associated 90% uncertainty range for the detectable signals, which are marked by an asterisk (*). Forcing fingerprints are centred to the period analyzed.

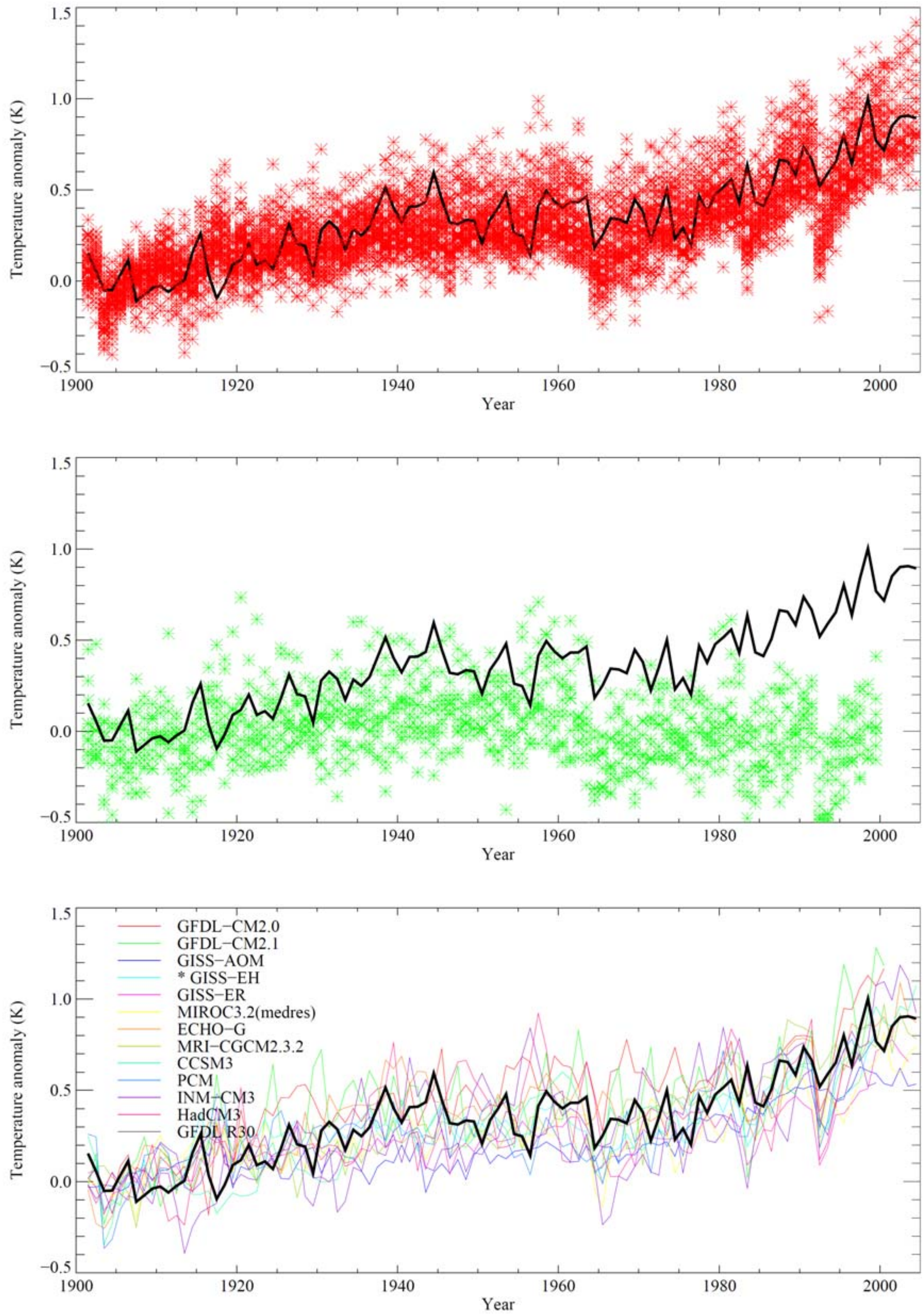

Figure 9.4.1. Global mean temperature as observed (black line) and as modelled by a range of climate models when the simulations include (a) both anthropogenic and natural forcings and (b) natural forcings only. Shown in (c) are single simulations including both anthropogenic and natural forcings from each of the 13 climate models shown. From Stott et al., 2005a and Stone et al., 2005a.

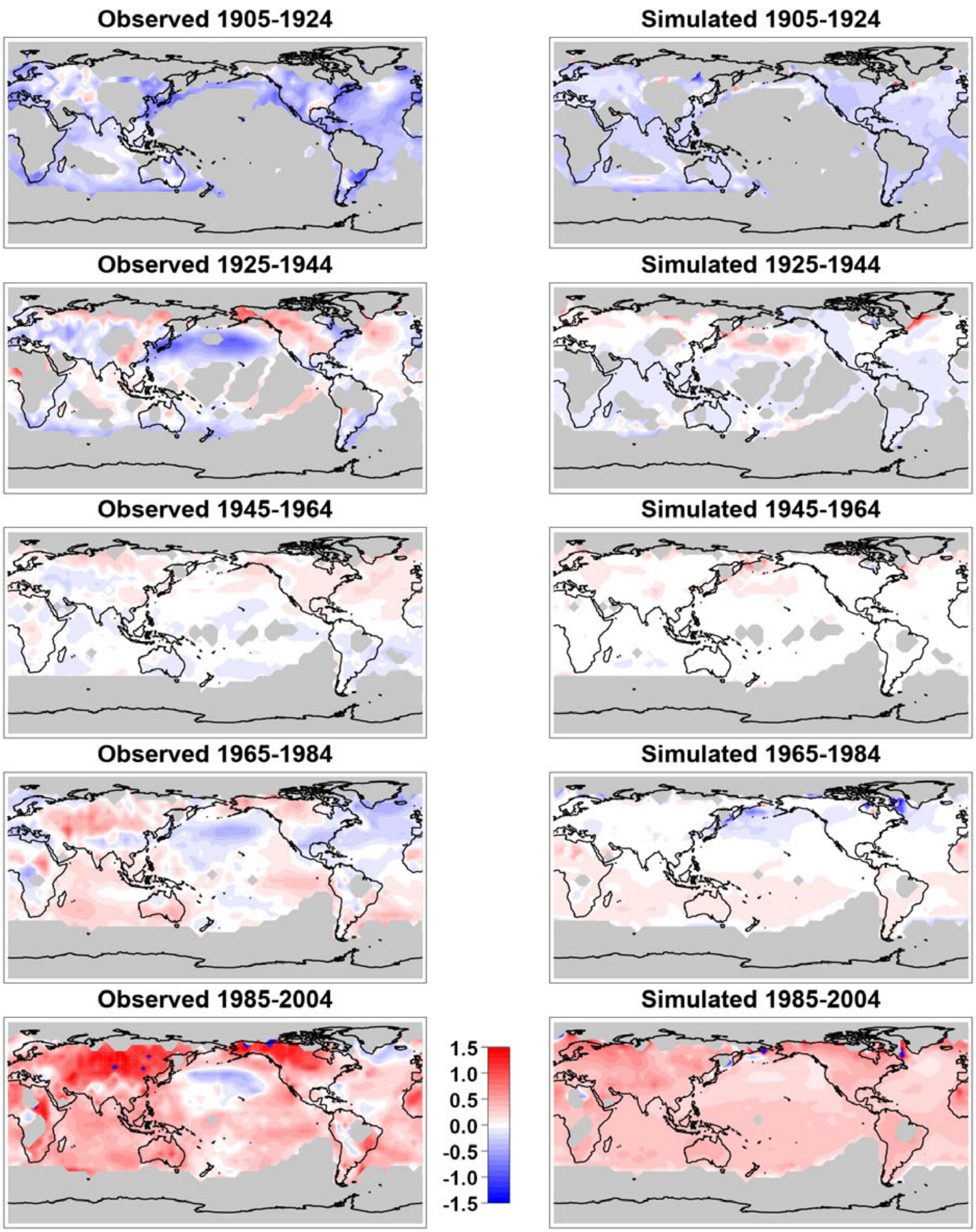

Figure 9.4.2. Bi-decadal mean temperature changes (°C) relative to 1945–1974 as observed and as modelled by the mean of 10 IPCC GCMs for five 20-year periods spanning the century 1905–2004. The 10 GCMs are the first 10 in the list given in Figure 9.4.1c.

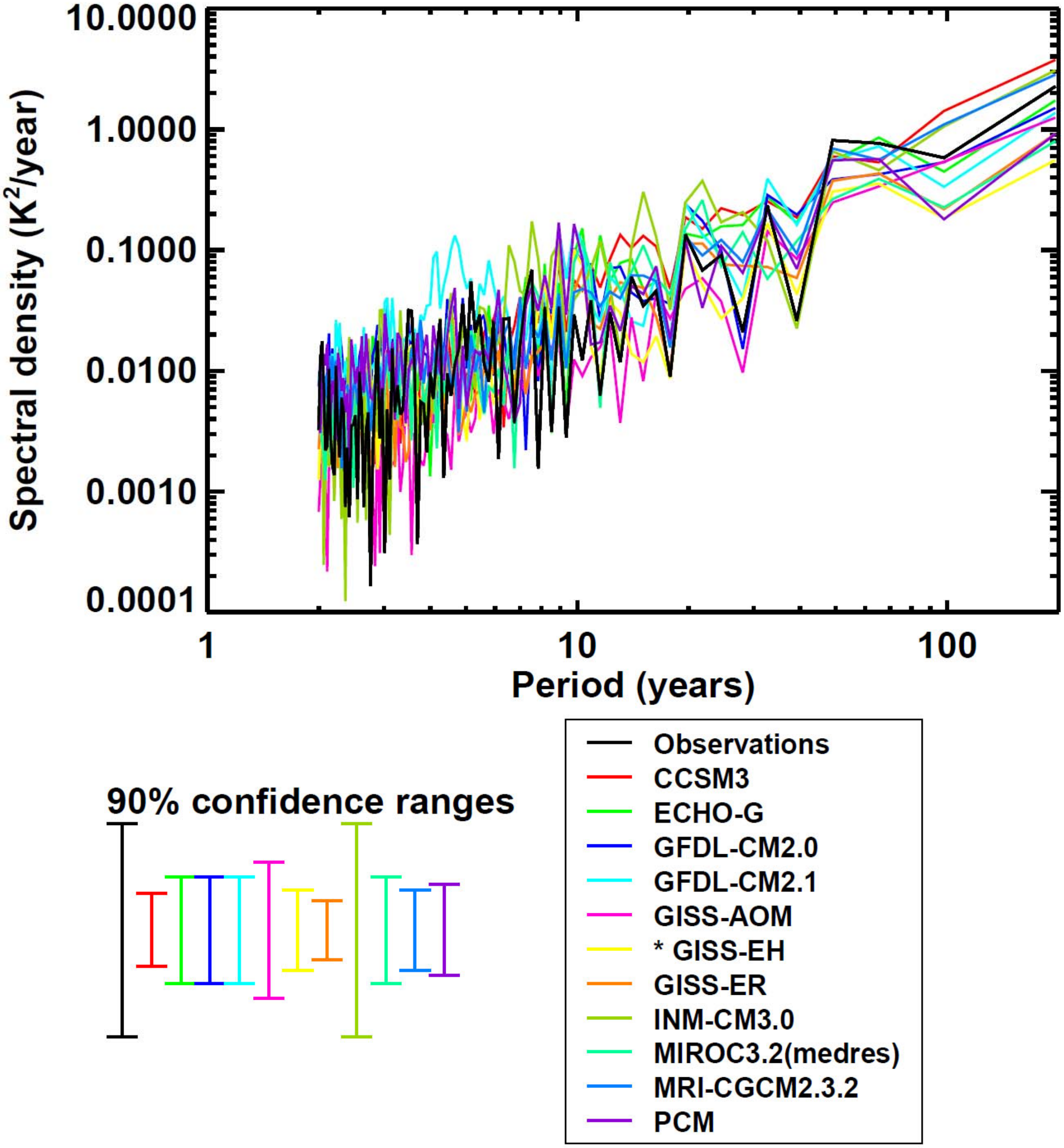

Figure 9.4.3. Power spectra of global mean temperatures from the observed record and from the ensemble means of coupled GCMs including both anthropogenic and natural forcings. GCMs marked by asterisks significantly over- or under- estimate the variability at time scales of 10 years and longer at the 10% level. All spectra are estimated using a Tukey-Hanning filter of width 98 years. From Stone et al., 2005a.

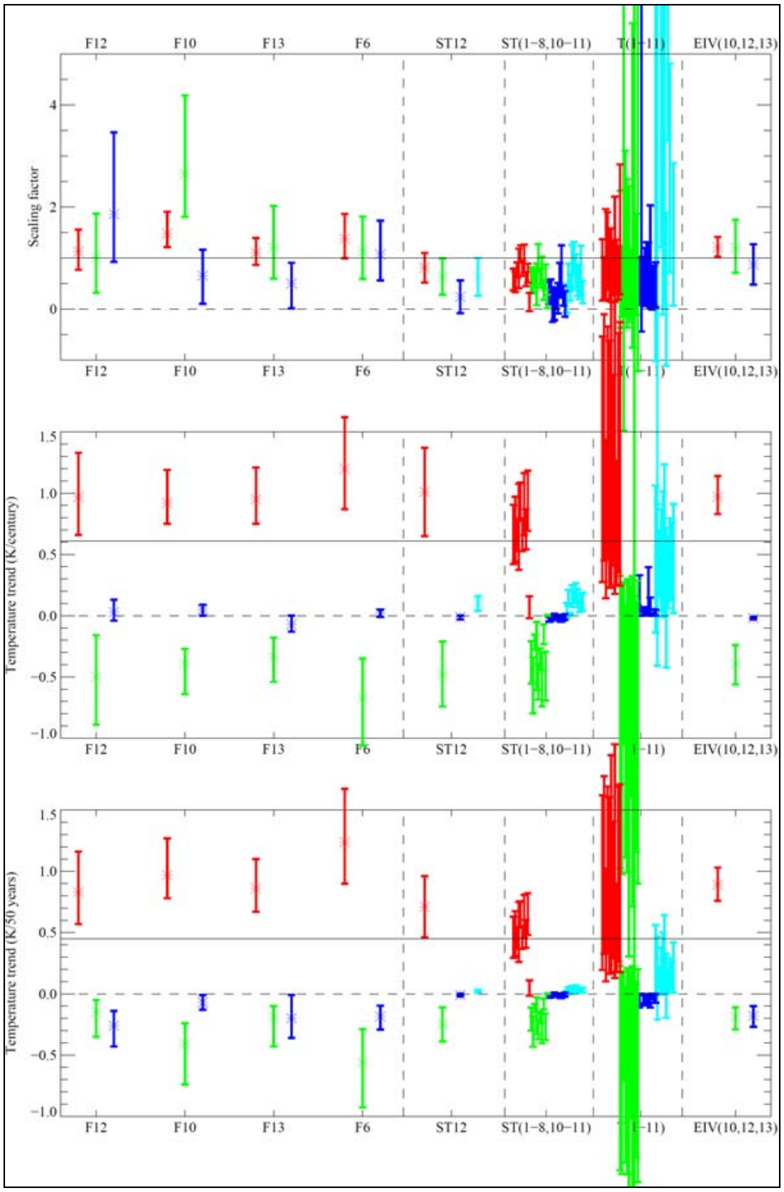

Figure 9.4.4. 5 to 95 percentile uncertainty limits on scaling factors (top) and reconstructed trends over the course of the 20th century (K/century) (center) and over 1950–1999 (K/50 years) (bottom) for the greenhouse gas (red), other anthropogenic (green) and natural (blue) components, based on detection analyses. Where only dark blue bars are shown, this refers to the total natural component and where dark blue and light blue bars are shown they refer to volcanic and solar contributions respectively. Labelled by F are the results of a full time-space optimal detection analysis (using a total least squares regression, Allen and Stott, 2003) from ensembles of simulations containing each set of forcings separately, labelled by T are results from an analysis based on temporal changes in global mean temperatures inferred from ensembles of all-forcings simulations of eleven coupled GCMs (the first eleven models in the list in Figure 9.4.1c and the same eleven models whose power spectra are shown in Figure 9.4.3; Stone et al., 2005b) and Energy Balance model approximations, and labelled by ST are results using a spatial-temporal analysis inferring patterns from all forcing runs for ten of the same eleven models. The uncertainty limits denoted EIV are from a combined analysis of spatio-temporal patterns of response from the HadCM3, PCM and GFDL R30 models for each of the three forcings separately, and incorporate inter-model uncertainty (Huntingford et al., 2005). The label is followed by numbers referring to the models (1 = GFDL CM2.0, 2 = GFDL CM2.1, 3 = GISS AOM, 4 = GISS EH, 5 = GISS-ER, 6 = MIROC3_2_MedRes, 7 = ECHO_G, 8 = MRI_CGCM2_3_2a, 9 = CCSM3, 10 = PCM, 11 = INM-CM3, 12=HadCM3, 13 = GFDL R30).

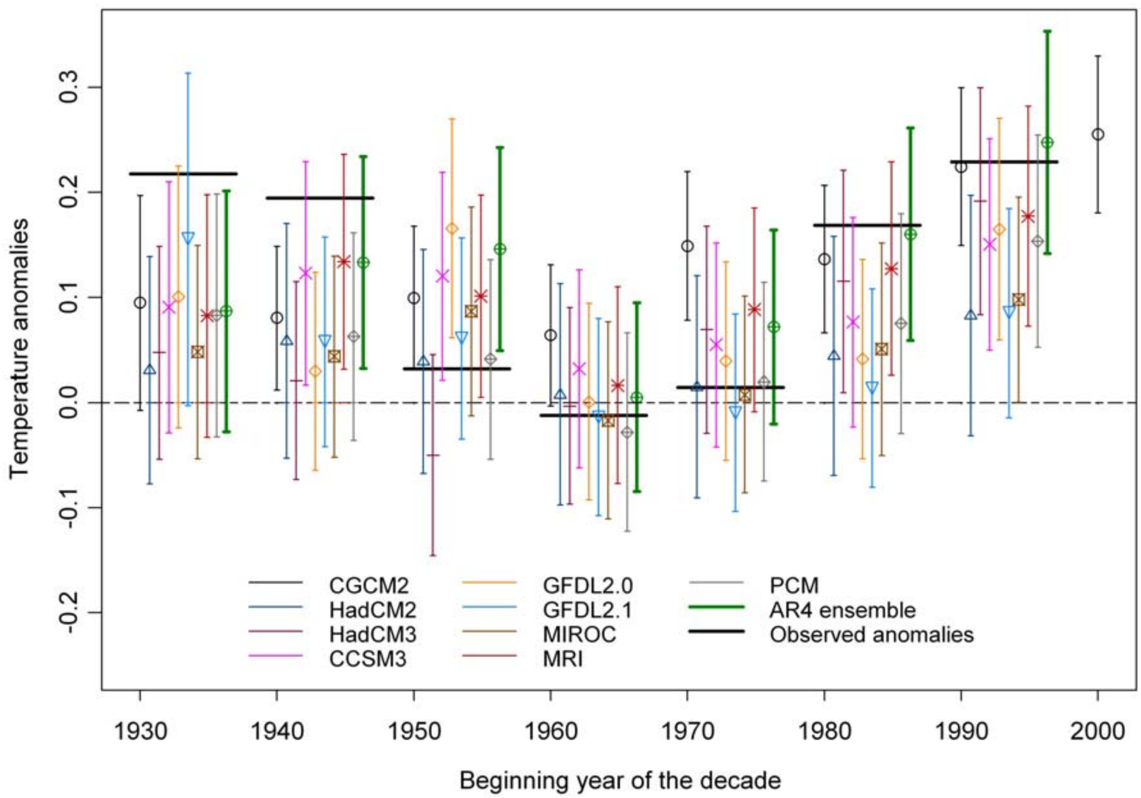

Figure 9.4.5. Hindcasts and their 5–95% confidence bounds of global decadal mean surface temperature anomalies relative to the preceding 30-year climatology made with models participating in IPCC AR4 C20C3M that have been forced with historical anthropogenic, and in some cases, natural forcings. Hindcasts based on the mean C20C3M model are indiced by the thick green line. Observed decadal anomalies are indicated by horizontal black bars. The hindcasts become generally skilful during the last two decades of the 20th century when anthropogenic forcing is large. A forecast for the decadal global mean anomaly for the decade 2000–2009, relative to the 1970–1999 climatology, based on simulations performed with the CCCma CGCM2 model is also displayed. Units are °C. After Lee et al. (2005b).

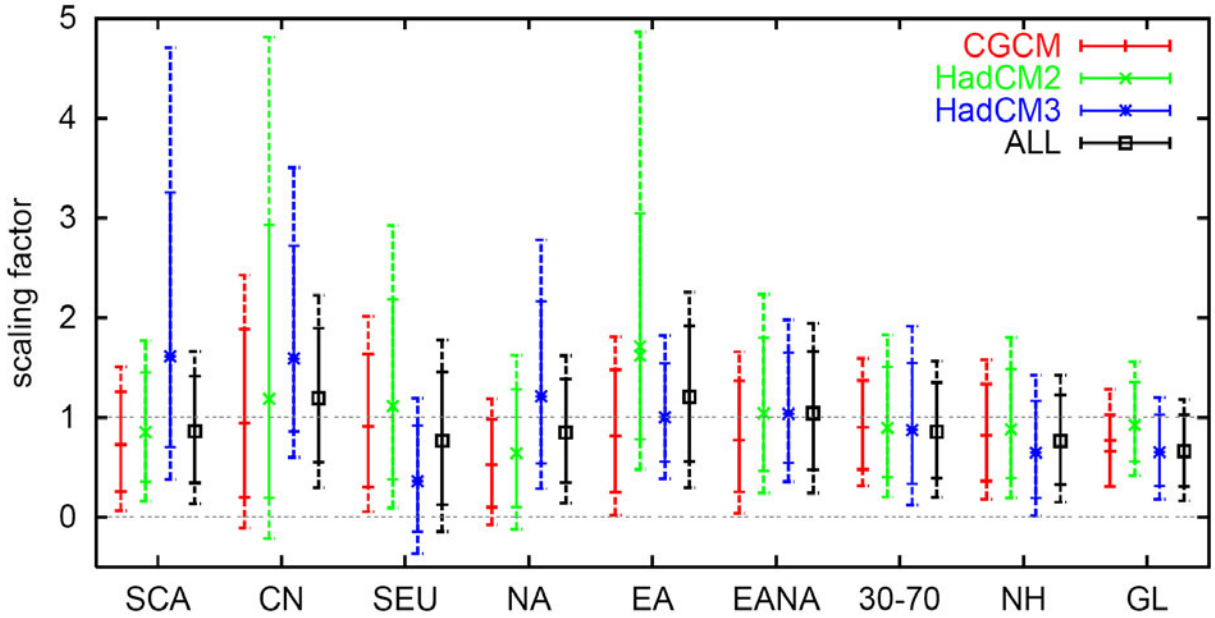

Figure 9.4.6. Scaling factors indicating the match between observed and simulated decadal near surface air temperature change (1950–1999) when greenhouse gas and aerosol forcing responses (GS) are taken into account in optimal detection analyses on a range of spatial scales (After Zhang et al., 2005; Hegerl et al., 2005c). Solid bars indicate 90% confidence intervals on the scaling factors, and the dashed extensions indicate the increased width of these confidence intervals when estimates of internal variability are doubled. Scaling factors and uncertainties are provided for different spatial domains including: Southern Canada (SCA, Canadian land area south of 70N), China (CN), Southern Europe (SEU, European land area over 10W–40E, 35–50N), North America Continent (NA, North America land area over 30N–70N), Eurasian Continent (EA, Eurasian continent over 30N–70N), mid-latitude land area (EANA, EA and NA combined), mid-latitude (over 30N–70N latitude band), Northern Hemisphere (NH), and the Globe (GL). The GS signals are obtained from CGCM1 and CGCM2 combined (labeled CGCM), HadCM2, and HadCM3

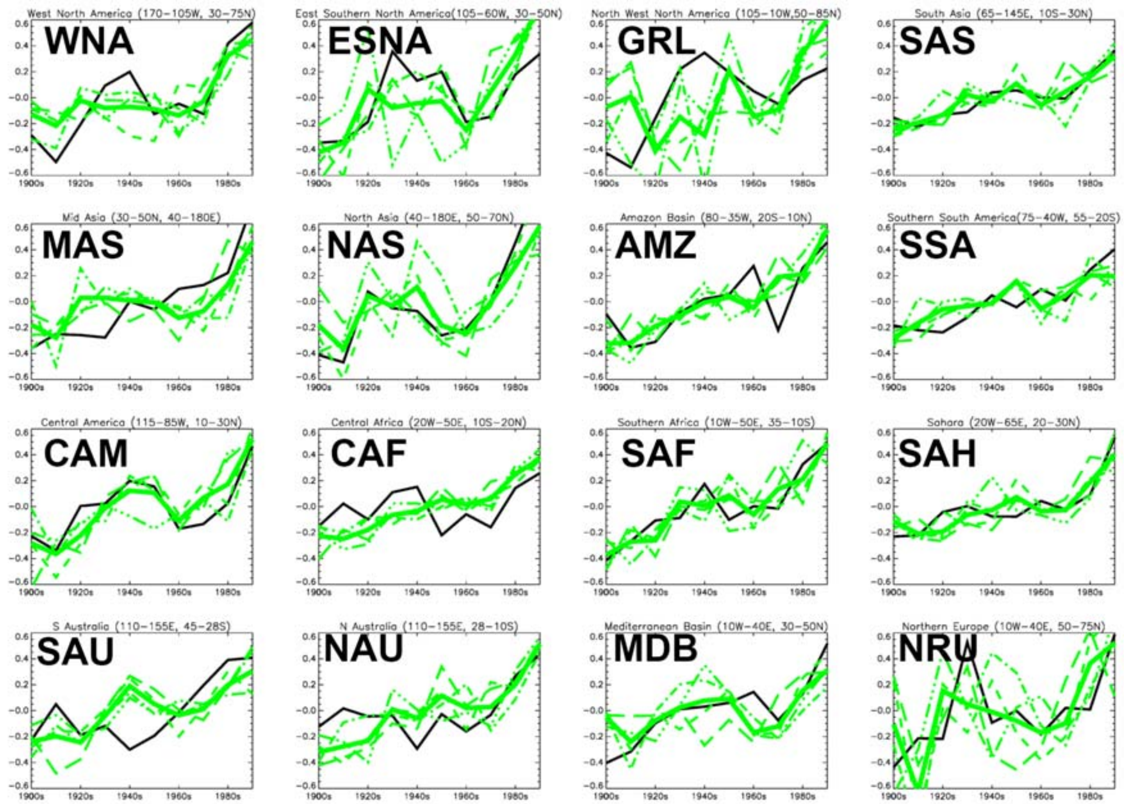

Figure 9.4.7. Comparison of HadCM3 all forcings runs with the observed decadal mean temperature changes in 1900–2000 for 16 sub-continental scale regions. The four dashed green curves represent the individual ensemble members, the solid green curve represents the ensemble mean, and observations are given in black. The model captures many features of the observed temperature changes, such as the steady warming in Southern Africa. Central America also has early and late century warming in both model and observations. North America is not particularly well captured with no early century warming in Western N. America in the model. South Australia is also not well captured. In mid Asia all model simulations suggest a cooling in the middle of the century while the observations show a general warming. Generally the model captures many features of both the variability and the trends in the different regions. The geographical domains of the regions are defined in Stott (2003, Table 1). From IDAG, 2004.

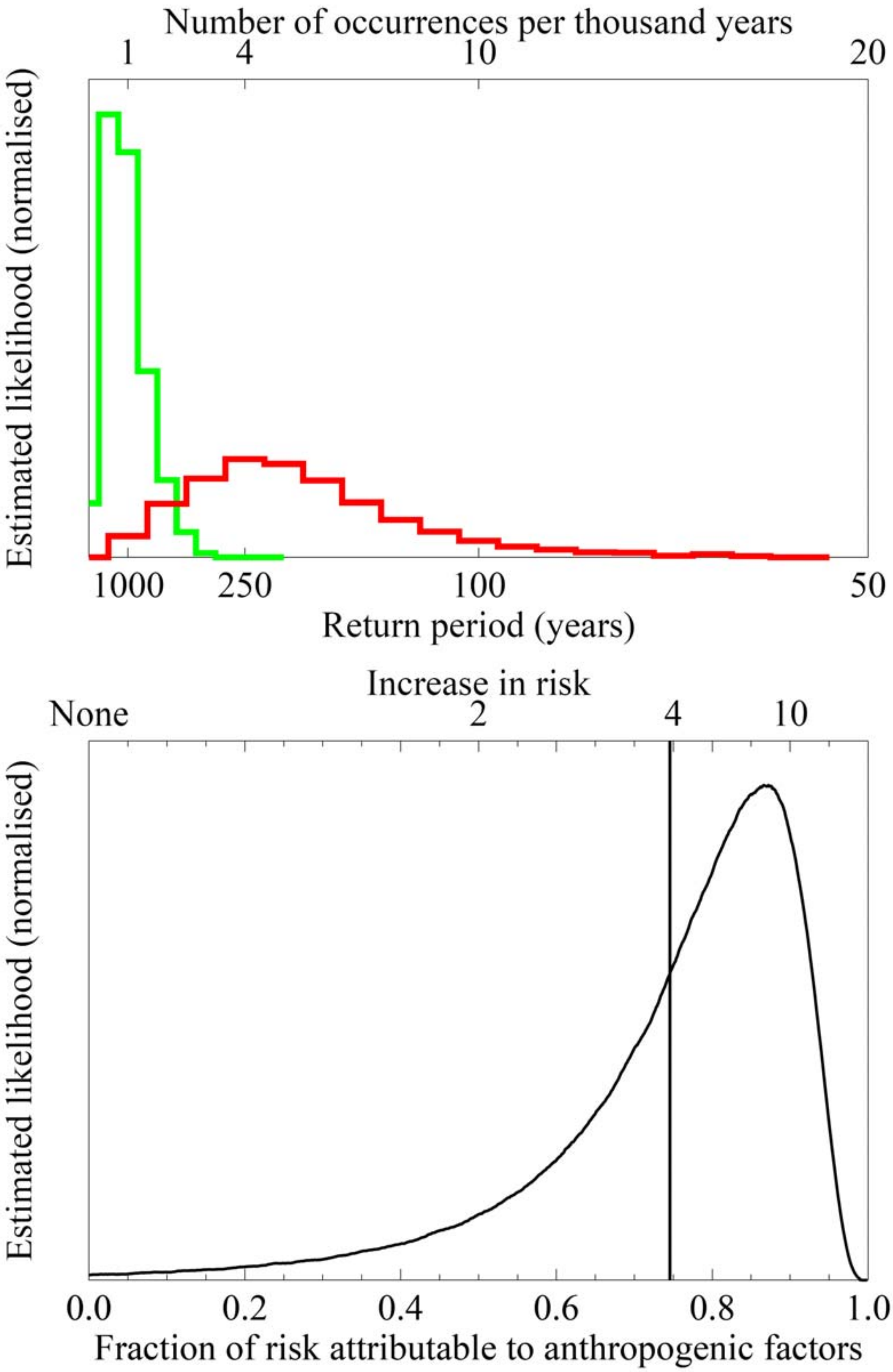

Figure 9.4.8. Change in risk of mean European summer temperatures exceeding the 1.6K threshold. a) Histograms of instantaneous return periods under late-twentieth-century conditions in the absence of anthropogenic climate change (green line) and with anthropogenic climate change (red line). b) Fraction attributable risk (FAR). Also shown, as the vertical line, is the “best estimate” FAR, the mean risk attributable to anthropogenic factors averaged over the distribution. From Stott et al., 2004.

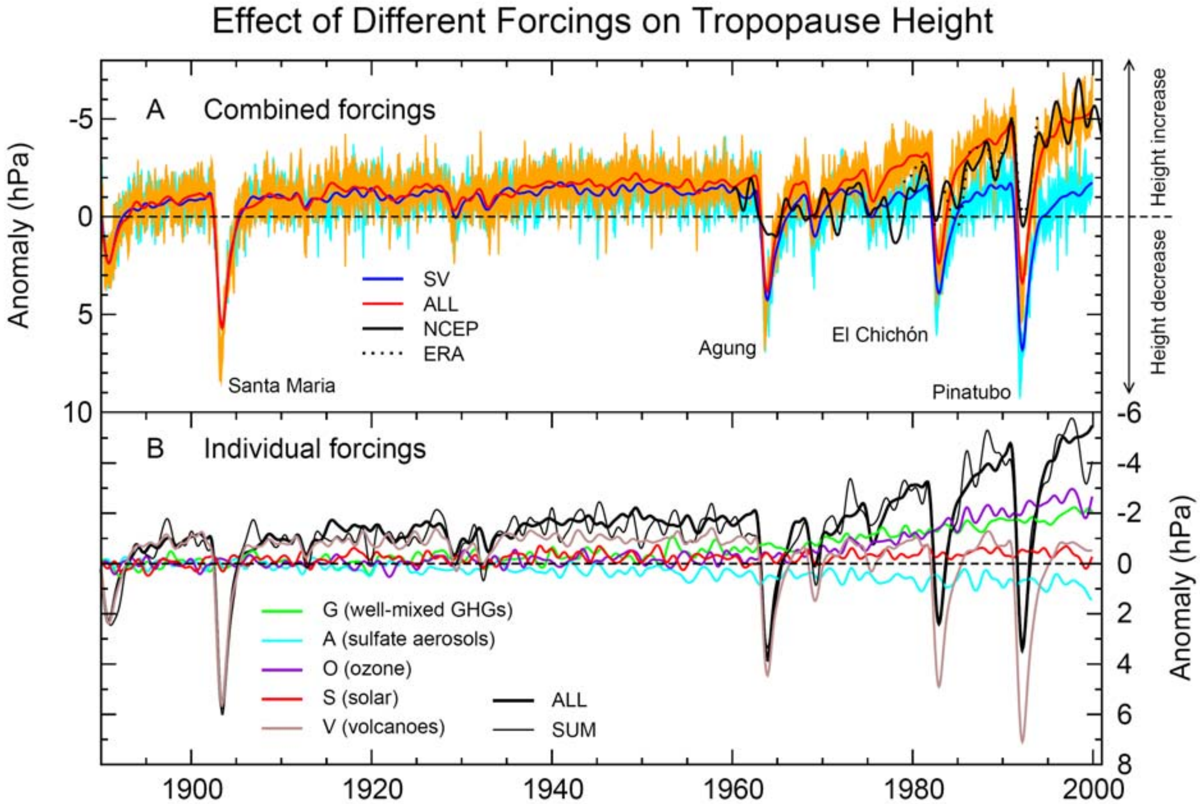

Figure 9.4.9. Time series of global mean monthly mean anomalies in tropopause pressure (pLRT). Model results are from seven different PCM ensemble experiments. Five experiments use a single forcing only (G, A, O, S, or V). Two integrations involve combined forcing changes, either in natural forcings (SV), or in all forcings (ALL). There are four realizations of each experiment. In B, only low-pass filtered ensemble means are shown. In A both the low-pass filtered ensemble mean and the (unfiltered) range between the highest and lowest values of the realizations are given. All model anomalies are defined relative to climatological monthly means computed over 1890–1999. Reanalysis based pLRT estimated from NCEP and ERA were filtered in the same way as model data. NCEP pLRT data are available from 1948–2001, but pre-1960 data were ignored because of deficiencies in the coverage and quality of assimilated radiosonde data. The ERA record spans 1979–1993. NCEP (ERA) was forced to have the same mean as ALL over 1960–1999 (1979–1993). The SUM results (B) are the sum of the filtered ensemble-mean responses from G, A, O, S, and V. From Santer et al. (2003b).

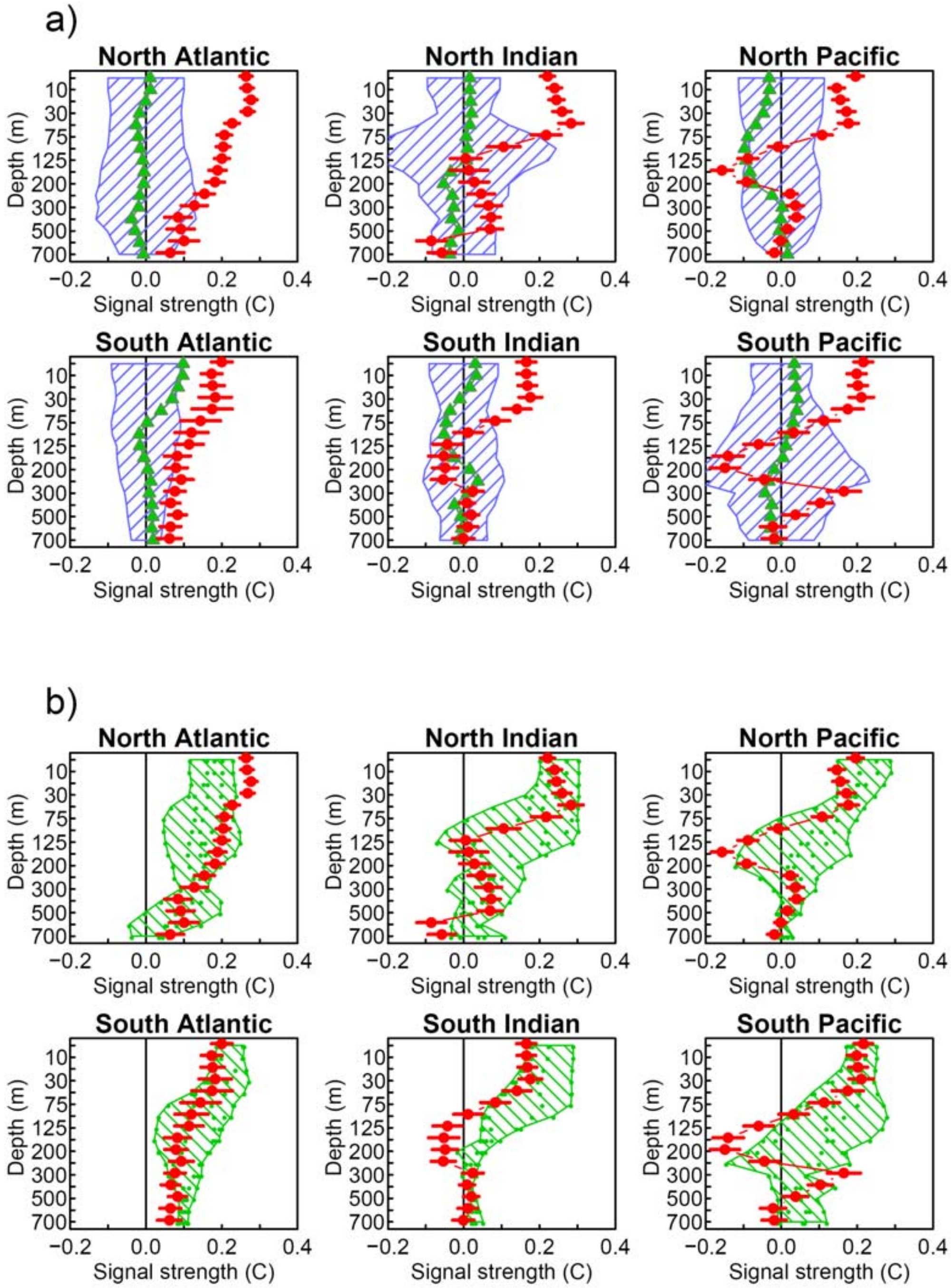

Figure 9.5.1. Warming signal strength by ocean and depth. (a) Comparison of observed changes and those expected from natural variability. The red dots represent the projection of the observed temperature changes onto the model-based pattern of warming. They show substantial basin-to-basin differences in how the oceans have warmed over the past 40 years, although all oceans have experienced net warming over that interval. The bars represent the ± two standard deviations limits associated with sampling uncertainty. The blue cross hatched swaths represent the 90% confidence limits of the natural internal variability strength. The ensemble averaged strength of the warming signal in four runs forced by solar and volcanic variability (green triangles) is also shown. The naturally forced signals are generally indistinguishable from those expected from natural internal variability alone. (b) Comparison of observed changes (red dots) and the anthropogenic forcing signal (green cross-hatched region). The hatched region shows the range of the signal estimates from five different realizations of identically forced simulations with the PCM model, while the smaller dots within the region are the individual realizations. (From Barnett et al., 2005)

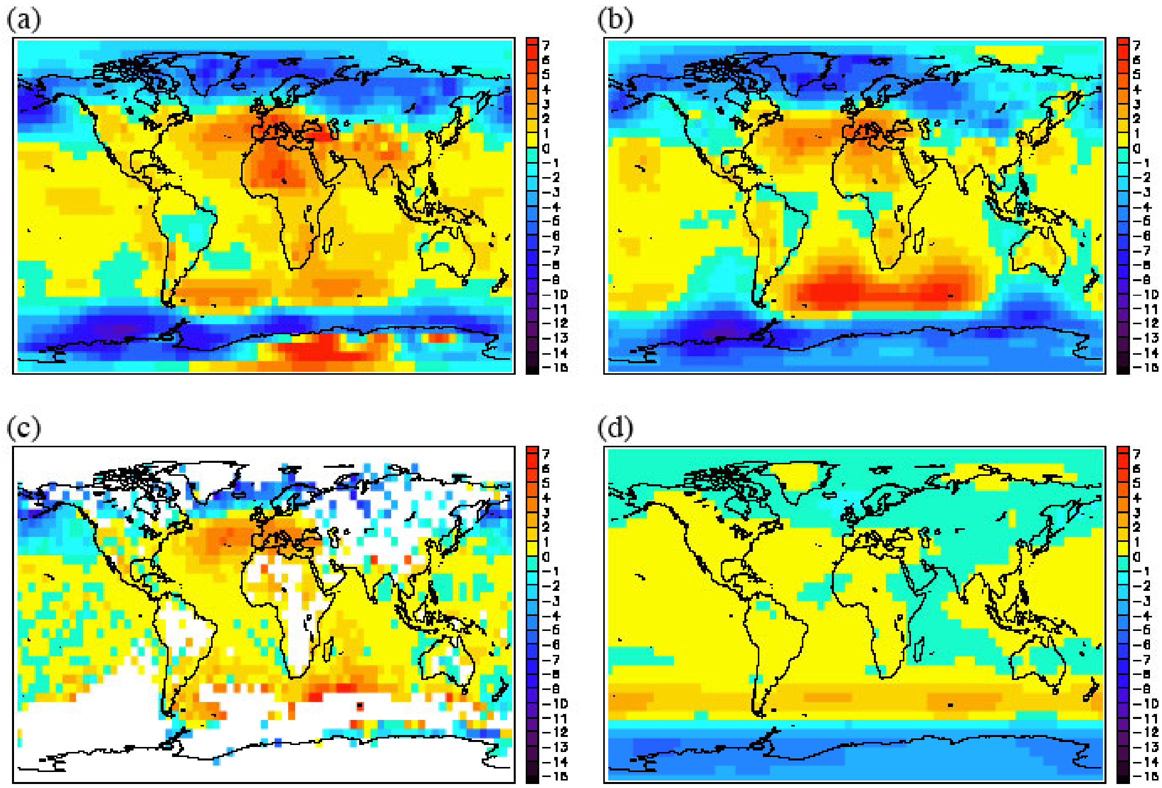

Figure 9.5.2. Observed and simulated sea level pressure trends. The December-February sea-level pressure trends based on decadal means for the period 1955–2005 are shown for (a) the NCEP-NCEP reanalysis, (b) the ERA-40 reanalysis, (c) the HadSLP2.0 dataset, and (d) the mean simulated response to greenhouse gas sulphate aerosol, stratospheric ozone, volcanic aerosol, and solar irradiance changes in eight IPCC AR4 coupled models (UKMO-HadCM3, CCSM3, PCM, GFDL-CM2.0, GFDL-CM2.1, MIROC3.2(medres), GISS-EH, GISS-ER). From Gillett et al. (2005**).**

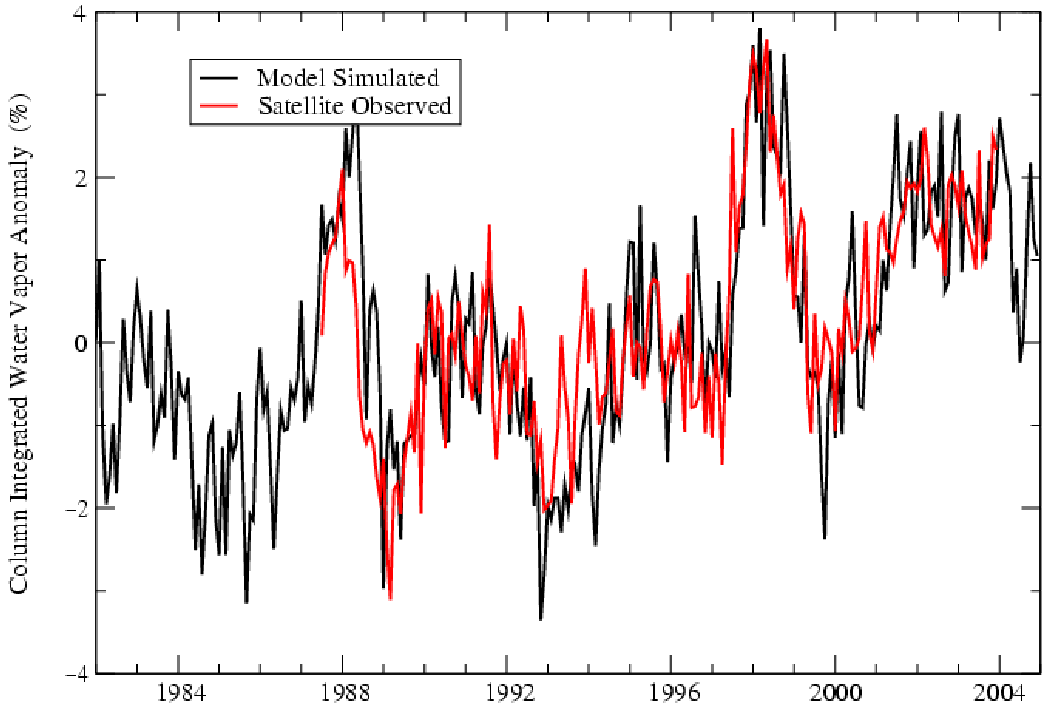

Figure 9.5.3. Global mean (ocean-only) anomalies in column integrated water vapour from GFDL atmospheric GCM simulations forced with observed sea surface temperatures (red), and satellite observations from SSMI (black). From Soden et al. (2005).

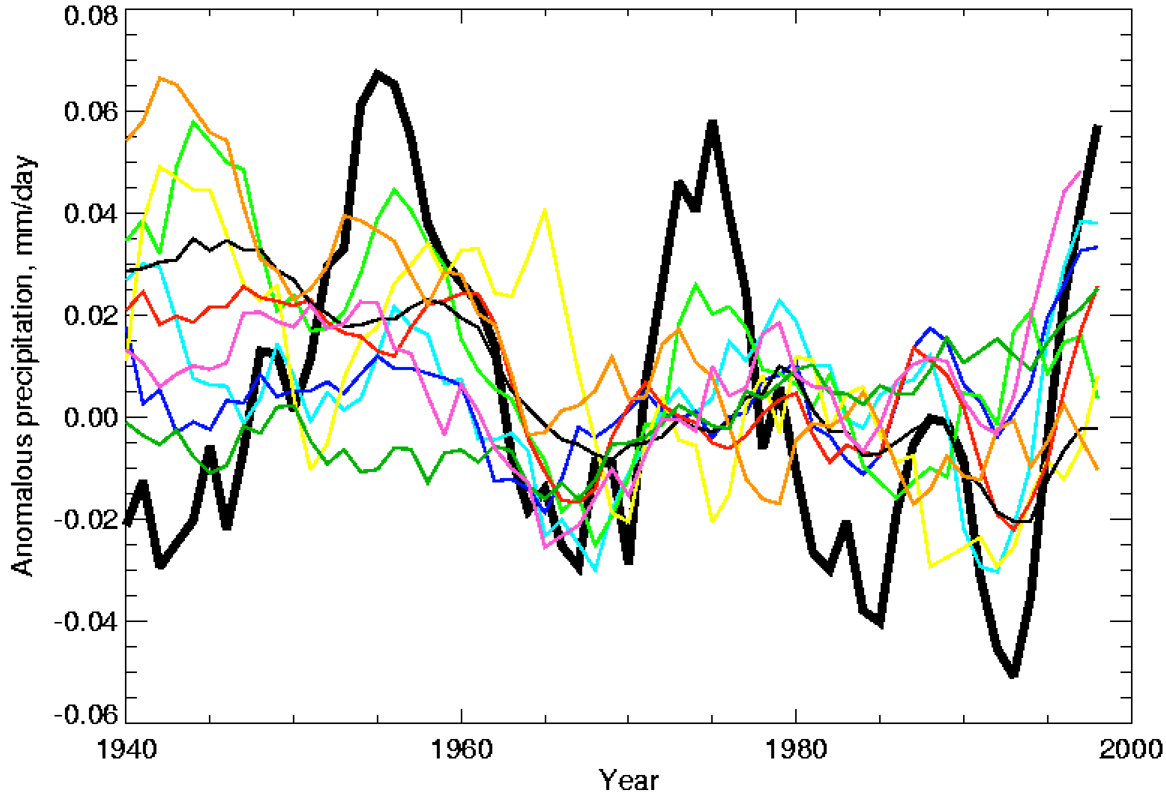

Figure 9.5.4. Simulated and observed anomalies in terrestrial mean precipitation. Observations are based on a gridded dataset of terrestrial rain gauge measurements (New et al., 2000) (thick black line). Model data are from 20th century integrations with anthropogenic, solar, and volcanic forcing from nine coupled climate models: UKMO-HadCM3 (pale blue), CCSM3 (dark blue), GFDL-CM2.0 (pale green), GFDL-CM2.1 (yellow), GISS-EH (red), GISS-ER (thin black), MIROC3.2 (orange), MRI-CGCM2.3.2 (dark green), and PCM (pink). A five year running mean was applied to suppress other sources of natural variability, such as ENSO. Adapted from Lambert et al., 2005.

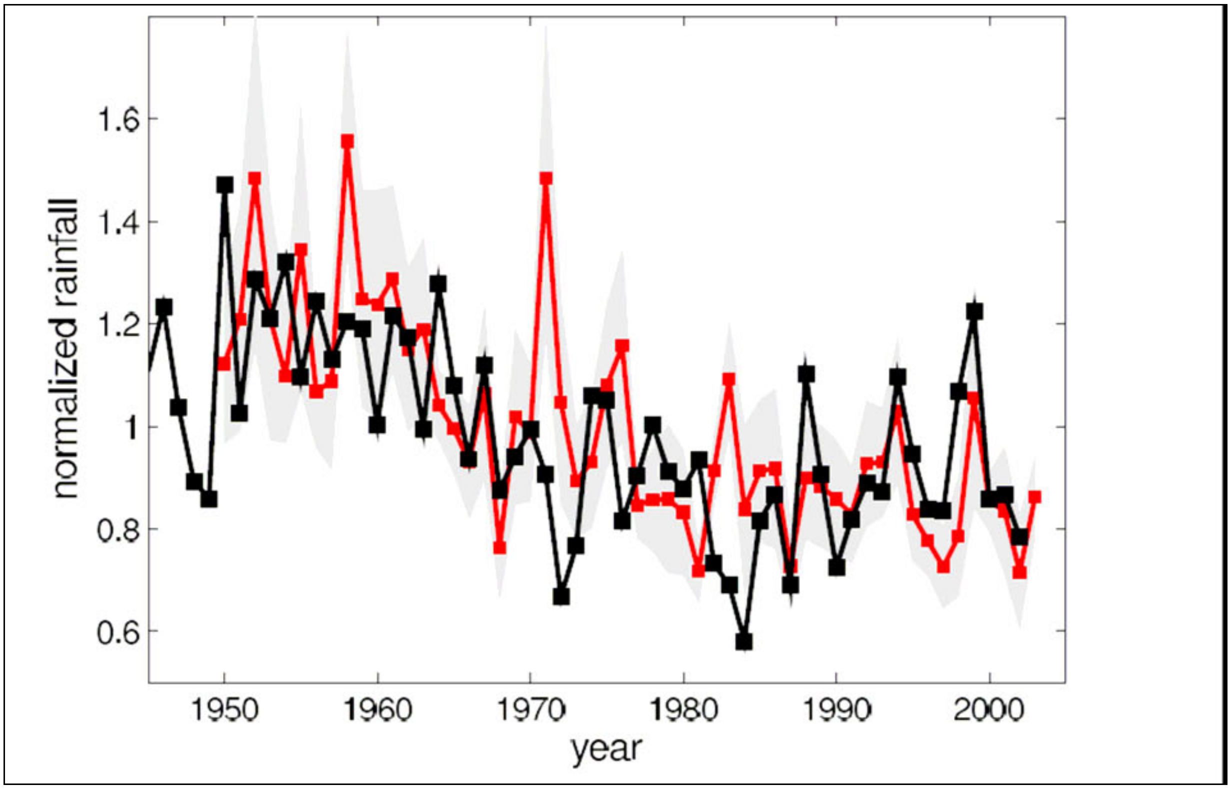

Figure 9.5.5. Observed (CRU) Sahel July-September rainfall for each year (black), and an ensemble mean of 10 simulations of the GFDL-CM2.0 model forced with observed SSTs. From Held et al. (2005).

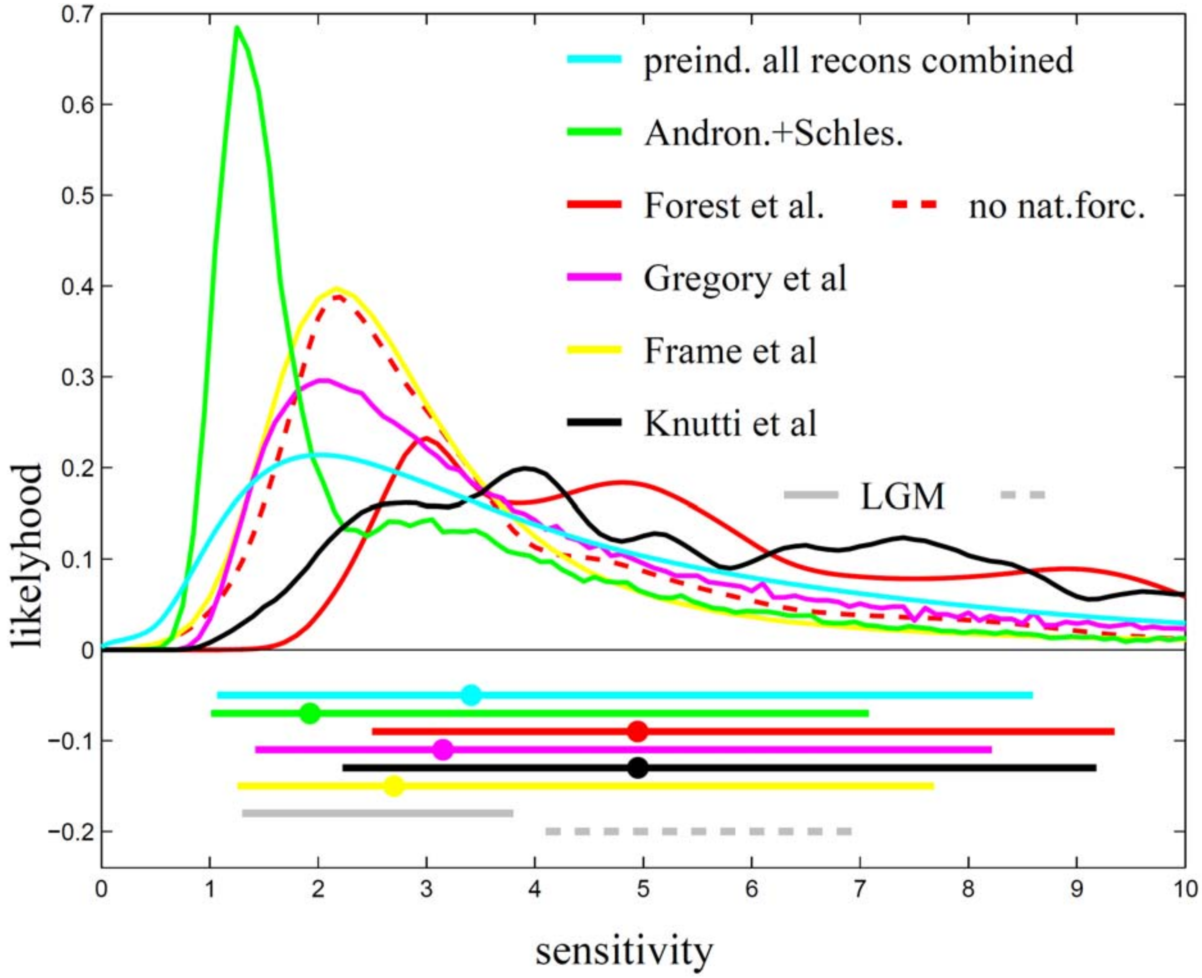

Figure 9.6.1. Comparison between different estimates of the probability density function (or relative likelihood) for equilibrium climate sensitivity. All PDFs/likelyhoods have been scaled to integrate to 1 between 0 and 10. The bars show the respective 5-95% ranges, dots the median estimate. Pdfs/likelihoods are from Andronova and Schlesinger, 2001; Forest et al., 2002 (dashed line, considering anthropogenic forcings only), Forest et al., 2005 (solid, anthropogenic and natural forcings), Gregory et al. (2002), Knutti et al. (2002), Frame et al. (2005), Hegerl et al. (2005b). Also shown are the 5–95% approximate ranges for two estimates from the Last Glacial maximum (solid: Schneider von Deimling et al., 2005; dashed: Annan et al., 2005), which are based on two different EMICs with different structural properties.

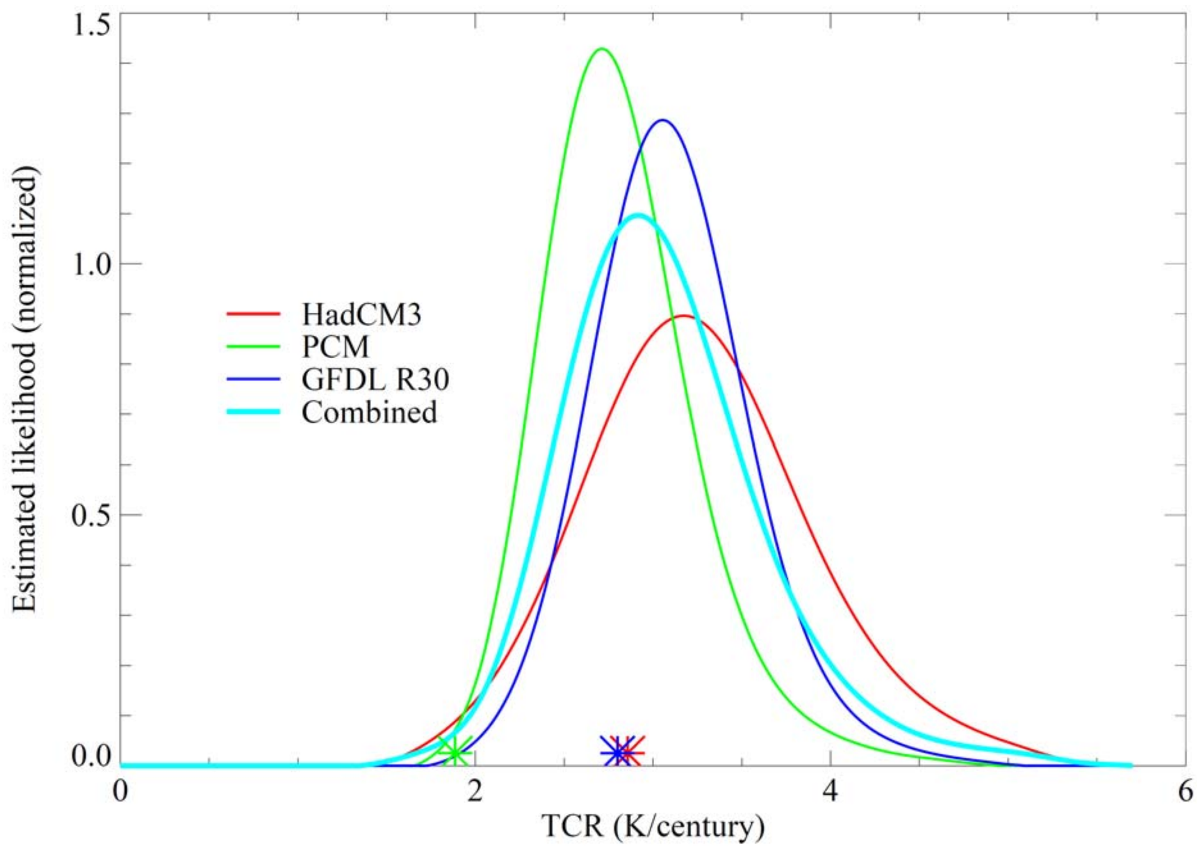

Figure 9.6.2. Probability distributions of transient climate response (expressed as warming rates over the century), as constrained by observed 20th century temperature change, for HadCM3 (red), PCM (green), GFDL R30 (blue) models and combining the PDFs derived from each model (turquoise). Coloured stars show each model's TCR. (From Stott et al., 2005c)